International Journal of Nanomedicine

Dovepress
open access to scientific and medical research

Open Access Full Text Article

ORIGINAL RESEARCH

Apoptotic Extracellular Vesicles from Supernumerary Tooth-Derived Pulp Stem Cells Transfer COL1A1 to Promote Angiogenesis via PI3K/Akt/VEGF Pathway

Yue Fei[1,2], Zhichen Ling[1,2], Qian Tong[1,2], Jun Wang[1,2]

[1]Department of Pediatric Dentistry, Shanghai Ninth People's Hospital, Shanghai Jiao Tong University School of Medicine, College of Stomatology, Shanghai Jiao Tong University, National Center for Stomatology, National Clinical Research Center for Oral Diseases, Shanghai Key Laboratory of Stomatology, Shanghai Research Institute of Stomatology, Shanghai, People's Republic of China; [2]Shanghai Engineering Research Center of Advanced Dental Technology and Materials, Shanghai, People's Republic of China

Correspondence: Jun Wang, Email wangjun202@126.com

Purpose: Angiogenesis is a tightly controlled process that initiates the formation of new vessels and its dysfunction can lead to life-threatening diseases. Apoptotic extracellular vesicles (ApoEVs) have emerged as a proangiogenic agent with high safety and isolation efficiency profile, and ApoEVs from supernumerary tooth-derived pulp stem cells (SNTSC-ApoEVs) have their unique advantages with an easily accessible parental cell source and non-invasive cell harvesting. However, the detailed characteristics of SNTSC-ApoEVs are largely unknown. This study aimed to investigate the proangiogenic capacity and function molecule of SNTSC-ApoEVs.

Methods: SNTSC-ApoEVs were isolated and characterized. In vitro effects of SNTSC-ApoEVs on the proliferation, migration, and tube formation of human umbilical vein endothelial cells (HUVECs) were evaluated by CCK-8, wound healing, transwell, and tube formation assays. The mRNA and protein levels of proangiogenic genes were quantified by qRT-PCR, Western blot, and immunofluorescence analysis. A Matrigel plug model was established in 6-week-old male nu/nu mice for one week, and the in vivo impact of SNTSC-ApoEVs on micro-vessel formation was assessed by histological analysis. Proteomic analysis and RNA sequencing were performed to explore the active ingredients and underlying mechanisms.

Results: SNTSC-ApoEVs enhanced the proliferation, migration, and angiogenesis of HUVECs in vitro. In the Matrigel plug model in vivo, SNTSC-ApoEVs promoted CD31-positive luminal structure formation. Apart from expressing general ApoEV markers, SNTSC-ApoEVs were enriched with multiple proteins related to extracellular matrix-cell interactions. Mechanistically, SNTSC-ApoEVs transferred COL1A1 to HUVECs and promoted endothelial functions by activating the PI3K/Akt/VEGF cascade.

Conclusion: SNTSC-ApoEVs can promote angiogenesis by transferring the functional molecule COL1A1 and activating the PI3K/Akt/VEGF pathway, making SNTSC-ApoEVs a promising strategy for the treatment of angiogenesis-related diseases.

Keywords: apoptotic extracellular vesicles, supernumerary tooth-derived stem cells, angiogenesis, COL1A1, PI3K/Akt pathway

Introduction

Angiogenesis is defined as the formation of new blood vessels from a pre-existing vascular network that naturally occurs in response to tissue injury.[1] Pathophysiological conditions can disrupt this process, resulting in numerous diseases such as stroke, ischemic heart disease, and chronic wounds. Therapeutic agents, including cytokines and exosomes, have been administered to alleviate ischemic damage.[2] However, high cost and increased cancer development risks limit the former approach,[3] while the latter one faces several challenges in isolation, preservation, and relatively low yield, making it less ideal for clinical translation.[4] Therefore, there is an urgent need for a new proangiogenic molecule that can overcome these limitations and effectively treat these debilitating diseases.

Received: 17 April 2024
Accepted: 21 June 2024
Published: 8 July 2024

Emerging evidence has revealed the crucial role played by apoptotic extracellular vesicles (ApoEVs) in tissue repair and regeneration.[5,6] Unlike regular extracellular vesicles generated by viable cells, ApoEVs represent all classes of subcellular vesicles produced as a consequence of apoptosis,[7] are derived from different biogenesis,[5] have larger volumes and a wider diameter distribution,[8] possess unique content and express specific apoptosis-related markers.[9] These heterogeneous nanosized vesicles, containing proteins, DNAs, RNAs, lipids, and metabolites secreted during apoptosis,[10] have been shown to contribute significantly to the neovascularization of crucial tissues such as the myocardium, skin, and endometrium.[7,11,12] ApoEVs boast numerous benefits, including low immunogenicity,[13,14] ease of separation, high yield, and no longer being subject to harsh preservation regulations,[15,16] making them ideal candidates for clinical applications.[17] However, despite their immense potential, the detailed proangiogenic components of ApoEVs remain poorly understood. Further investigation of these remarkable vesicles is crucial in unlocking their full potential in clinical settings.

Recent research has shown that apoptotic mesenchymal stem cells (MSCs) release more ApoEVs than other cells types.[18] Candidate MSCs sources of ApoEVs include human bone marrow MSCs (BMMSCs), human adipose-derived MSCs (ADMSCs), human umbilical cord-derived MSCs, human embryonic stem cells, human deciduous pulp stem cells, rat BMMSCs, and rat ADMSCs.[10–12,15,19–21] Among these MSCs, only human deciduous pulp stem cells can be harvested from exfoliated deciduous teeth in an non-invasive way.[22] However, root resorption of deciduous teeth may lead to insufficient cell number or low proliferative capacity,[23] which increases the difficulty in harvesting human deciduous pulp stem cells. Moreover, only few studies have explored the molecular mechanisms of MSC-ApoEVs-induced vascularization. ApoEVs from human deciduous pulp stem cells and rat BMMSCs have been found to activate endothelial autophagy via the transcription factor EB-autophagy pathway,[12,20] while ApoEVs from rat ADMSCs induced M2 polarization of macrophages via miR-21-5p transfer and enhanced angiogenesis of dermal microvascular endothelial cells.[21] Considering the heterogeneity of ApoEVs, their underlying proangiogenic mechanisms may involve multiple pathways and require further exploration.

A newly discovered population of MSCs, called supernumerary tooth-derived pulp stem cells (SNTSCs), has been identified from the dental pulp of human supernumerary teeth which are usually extracted and discarded clinically, and their paracrine capability has been reported.[24,25] SNTSCs not only share similar non-invasive sampling characteristic to human deciduous pulp stem cells, these MSCs may also be more accessible since supernumerary teeth have an incidence of 2.4%-6% and contain pulp tissue with larger size, weight than deciduous teeth,[25,26] making them a promising stem cell source to produce ApoEVs. Nevertheless, the detailed characteristics of ApoEVs from SNTSCs (SNTSC-ApoEVs) and the mechanisms of their actions are unclear.

In this study, we isolated SNTSC-ApoEVs and tested their proangiogenic capacity in vitro. Matrigel plug assay, an in vivo model for assessing neovascularization, was used to demonstrate the robust ability of SNTSC-ApoEVs to promote micro-vessel formation. Through a series of proteomic and transcriptional profiling analyses, we provided mechanistic insights into SNTSC-ApoEVs. These analyses revealed the enrichment of multiple proteins within SNTSC-ApoEVs, with COL1A1 emerging as the primary factor involved in promoting angiogenesis and PI3K/Akt/VEGF pathway being the major pathway corresponding to enhanced endothelial functions. These findings contribute to a more comprehensive understanding of ApoEVs from dental stem cells and pave the way for their therapeutic application in diseases associated with inadequate angiogenesis.

Materials and Methods

Mice

All animal experimental procedures were conducted following the Laboratory animals-General code of animal welfare guidance (GB/T 42011–2022) and approved by the Laboratory Animal Ethics Committee in Shanghai Ninth People's Hospital Affiliated to Shanghai Jiao Tong University School of Medicine (No. SH9H-2022-A944-1). Nu/nu mice were obtained from Gempharmatech (China) and used to establish a Matrigel plug model.

Cell Culture

The cells used in this study and the relevant experiments were approved by the Medical Ethics Committee in Shanghai Ninth People's Hospital Affiliated to Shanghai Jiao Tong University School of Medicine (No.SH9H-2021-T66-1). After obtained the consent from the patients' parents, supernumerary teeth were collected from 3 children aged 5–7 years old. SNTSCs were isolated from the single donated tooth according to previously reported method.[27] The cells were cultured in DMEM supplemented with 10% fetal bovine serum (Gibco, USA), 100 U/mL penicillin-G, and 100 mg/mL streptomycin (Roche, Switzerland), and maintained in a 5% CO_2 atmosphere at 37°C. Cells at passages P3-P4 were used in this study.

Flow cytometric analysis was performed to detect surface markers using the following fluorescein isothiocyanate-conjugated anti-human monoclonal antibodies (BD Biosciences, USA): anti-CD34-FITC, anti-CD44-allophycocyanin -APC, anti-CD45-APC, anti-CD73-APC, anti-CD90-phycoerythrin-PE-, anti-CD105-PE, and anti-HLA-DR-PE. To induce multi-lineage differentiation, SNTSCs were separately cultured in osteogenic, adipogenic, and chondro-inductive media obtained from Cyagen Biosciences (China). Once the predetermined time point was reached, the samples were stained with Alizarin red, oil red O, and Alcian blue, as previously described.[28]

Human umbilical vein endothelial cells (HUVECs) were obtained from Beijing Zhongyuan Limited (China), and cultivated in α-MEM (Biosharp, China) supplemented with 10% fetal bovine serum (Gibco, USA), 100 U/mL penicillin-G and 100 mg/mL streptomycin (Roche, Switzerland).

Isolation of SNTSC-ApoEVs

When SNTSCs reached full confluence, they were washed with PBS and cultured in basic medium containing 10% EV-depleted FBS and 500 nM staurosporine (STS; Aladdin, China) for 16 h. Apoptosis was detected by morphological observation using an Olympus FV3000 digital microscope and a terminal deoxynucleotidyl transferase-mediated dUTP nick end labeling (TUNEL) assay (BL645B, Biosharp, China) according to the manufacturer's protocol. SNTSC-ApoEVs were then isolated from culture supernatant and purified as previous reported.[19] Briefly, after 800×g centrifugation for 10 min and 2000×g centrifugation for 10 min to remove cell debris, the supernatant was subsequently centrifuged at 16,000×g for 30 min to pellet the SNTSC-ApoEVs. The precipitate was collected and washed twice with PBS.

Characterization of SNTSC-ApoEVs

The morphology of SNTSC-ApoEVs was observed using transmission electron microscope (TEM). SNTSC-ApoEV pellets were resuspended in 2.5% glutaraldehyde and then dripped onto 200-mesh Formvar-coated copper grids. After washing, samples were negatively stained with 2.5% uranyl acetate for 2 min. Images were captured using a JEM-1200EX TEM. The size distribution of SNTSC-ApoEVs was measured using nanoparticle tracking analysis (NTA) with NanoSight NS300 system (NanoSight Technology, UK). Furthermore, BCA protein assay (Invitrogen, USA) was used to quantify protein concentration. The expressions of Caspase-3 and Cleaved Caspase-3 were detected by Western blot. For phosphatidylserine (PtdSer) detection, SNTSC-ApoEVs were suspended in 195 μL PBS and 5 μL FITC Annexin V (Beyotime, China) was added to incubate at room temperature for 15 min. Images were captured by confocal microscopy (FV1000, Olympus, Japan) after smear.

Internalization of SNTSC-ApoEVs into HUVECs in vitro

The HUVECs were seeded in dishes and maintained at 37°C overnight. SNTSC-ApoEV pellets were pre-labeled with PKH26 (Sigma-Aldrich, USA) according to the manufacturer's instructions, washed twice with PBS, and centrifuged at 16,000 × g for 30 min. PKH26-labeled SNTSC-ApoEVs at a concentration of 25 μg/mL were then co-cultured with HUVECs for 8 h. After fixed with 4% paraformaldehyde for 30 min at room temperature, the cytoskeleton was stained with phalloidin-fluorescein staining (Yeasen, China) and the cell nuclei were counter-stained with Hoechst 33342 (Sigma-Aldrich, USA). Fluorescent images were obtained with a laser scanning confocal microscope (FV1000, Olympus, Japan).

CCK-8 Assay

The proliferative capacity of HUVECs was evaluated using the CCK-8 assay. HUVECs (5×10^3 cells per well) were seeded in 96-well plates until complete adherence and were pretreated with different doses of SNTSC-ApoEVs or an equal volume of PBS for 24 h. Then, the culture medium was replaced with α-MEM medium supplemented with 1% FBS. At 1,2,3 days, 10 μL of the Cell Counting Kit-8 (Biosharp, China) was added to each well. The 96-well plates were subsequently incubated at 37°C for 2 h and the absorbance at 450 nm was measured using BIO-TEK microplate reader.

Wound Healing Assay

HUVECs (3×10^5 cells/well) were seeded in 6-well plates and cultured in α-MEM medium until confluent monolayers were obtained. A linear wound was created using a 200 μL pipette tip. After washed with PBS, SNTSC-ApoEVs or PBS were added to serum-free α-MEM medium. The scratch area was measured at 0 h and 12 h using six representative images. The closure rate was calculated as follows: Closure percentage (%) = 100 – (scratch area at 12 h)/(scratch area at 0 h) ×100.

Transwell Assay

A transwell system with an 8 μm pore diameter (BD Falcon, USA) was used to evaluate vertical migration ability. HUVECs (2×10^5 cells/mL) were starved overnight, resuspended in serum-free α-MEM medium, and seeded in the upper chamber. Fresh serum-free medium with PBS (control) or SNTSC-ApoEVs was added to the lower transwell chamber. After incubated at 37°C for another 24 h, HUVECs passing through the upper chamber were fixed with 4% paraformaldehyde, stained with crystal violet (Biosharp, China), photographed with an inverted microscope (Olympus, Japan), and counted in five representative fields for quantification with ImageJ software.

Tube Formation Assay

In vitro capillary network formation was determined using a tube formation assay with Matrigel (354248, Corning, USA). HUVECs were pretreated with PBS (control) or different concentrations of SNTSC-ApoEVs for 24 h, and then seeded in Matrigel-coated wells of a 96-well plate at a density of 5×10^4 cells/well. Tube formation was recorded at 0 h and 6 h using an inverted microscope (Leica, Germany). The number of network structures in randomly selecting 5 fields per well was quantified using the ImageJ software.

Quantitative Real Time-Polymerase Chain Reaction Analysis (qRT-PCR)

For gene expression analysis, total RNA was extracted using TRIzol reagent (Invitrogen, USA), and one microgram of total RNA was reverse-transcribed into cDNA with First-strand cDNA Synthesis Kit (Yeasen, China). SYBR Green Kit (Takara Bio, Japan) and LightCycler 480 Real-Time PCR System (Roche, USA) were used for cDNA amplification. The results were analyzed with the $2^{-\Delta\Delta CT}$ relative quantitative method. β-actin was used as an internal control. Gene expression was normalized to internal control. The primer sequences used are listed in Table 1.

In vivo Matrigel Plug Assay

6-week-old male nu/nu mice weighing 16–18 g were used to establish a Matrigel plug model. HUVECs pretreated with normal or SNTSC-ApoEVs-supplemented mediums for 24 h were encapsulated in growth factor-reduced Matrigel (Corning, USA). After the mice were sedated with ketamine-xylazine (75 mg/kg, Gutian Pharma Co., China; 20 mg/kg, Sigma-Aldrich Chemical, USA), two groups of 500 μL HUVEC-Matrigel suspension were randomly injected subcutaneously into the bilateral flanks with one plug per side and formed a gel rapidly. After 7 days, blood chemistry examinations were performed, the mice were euthanized by CO_2 inhalation and Matrigel plugs were harvested and fixed with 4% PFA for 24 h. The tissues were subjected to histological analysis.

Table 1 Primer Sequences for qRT-PCR

Primers	Abbreviations	GenBank Accession	Sequences	
Vascular endothelial growth factor A	VEGFA	NM_001171627	Forward	AGGGCAGAATCATCACGAAGT
			Reverse	AGGGTCTCGATTGGATGGCA
Platelet endothelial cell adhesion molecule 1	PECAM1 (CD31)	NM_000442	Forward	CCAAGCCCGAACTGGAATCT
			Reverse	CACTGTCCGACTTTGAGGCT
Kinase insert domain receptor	KDR	NM_002253	Forward	GGCCCAATAATCAGAGTGGCA
			Reverse	CCAGTGTCATTTCCGATCACTTT
Collagen type I alpha 1 chain	COL1A1	NM_000088	Forward	CAGGGCGACAGAGGCATAAA
			Reverse	GGGAGACCGTTGAGTCCATC
β-actin	NA	NM_001101	Forward	TGGCACCCAGCACAATGAA
			Reverse	CTAAGTCATAGTCCGCCTAGAAGCA

Histological Analysis

The harvested tissues were dehydrated, embedded in paraffin, and sliced into 5 μm-thick sections. Hematoxylin and eosin (H&E) staining was conducted using an H&E staining kit (Solarbio, China), according to the manufacturer's instructions. For immunohistochemical staining, the sections were incubated with CD31 primary antibody (1:800, Cell Signaling Technology, #3528) overnight at 4°C before treatment with secondary antibody and DAB substrate. For immunofluorescence staining, sections were incubated with anti-CD31 (1:800, Cell Signaling Technology, #3528) overnight and processed with the secondary antibodies Alexa Fluor 594 AffiniPure Goat anti-mouse IgG secondary antibody (Yeasen, China) for 60 min. Images were captured using a Zeiss Axioscope 5 microscope and analyzed with ImageJ software.

Proteomic Analysis

SNTSC-ApoEV samples from three donors were used for proteomic analysis. Protein lysates were prepared and subjected to nano-LC-MS/MS analysis following protocols described in previous reports.[29] For proteomic analysis, timsTOF Pro2 (Bruker) was used to acquire mass spectrometry (MS) data in data-dependent acquisition in parallel accumulation-serial fragmentation (DDA PaSEF) mode. Raw vendor MS files were processed using SpectroMine software (4.2.230428.52329) and the built-in Pulsar search engine. The MS spectral lists were searched against their species-level UniProt FASTA databases (UniProt-Homo sapiens_9606-2022-11. FASTA); carbamidomethyl [C] as a fixed modification; and oxidation (M) and acetyl (Protein N-term) as variable modifications. Trypsin was used as protease. A maximum of two missed cleavages was allowed. The false discovery rate (FDR) was set to 0.01 for both PSM and peptide levels. All other parameters were reserved as default. Proteins enriched in both the samples (PG. Label-Free Quant > 0) were included for further functional analysis based on the Gene Ontology (GO) and Kyoto Encyclopedia of Genes and Genomes (KEGG) databases. Additionally, a protein-protein interaction (PPI) network was constructed using Cytoscape 3.6.1. Key hub proteins were identified by PPI network analysis using STRING database. The details of all the identified proteins are listed in Table S1.

RNA Sequencing (RNA-Seq)

HUVECs were grown on glass coverslips until confluence and treated with SNTSC-ApoEVs or PBS for 24 h. Total RNA was extracted using the TRIzol reagent (15596018, Thermo Fisher Scientific). Total RNA (5μg) was qualitied and purified with Bioanalyzer 2100 and RNA 6000 Nano LabChip Kit (5067–1511, Agilent), and high-quality RNA samples with RIN number > 7.0 were used to construct the sequencing library. Following purification, the mRNA was fragmented and reverse-transcribed with SuperScript™ II Reverse Transcriptase (1896649, Invitrogen), which was then used to synthesize U-labeled second-stranded DNAs using E. coli DNA polymerase I (m0209, NEB), RNase H (m0297, NEB), and dUTP solution (R0133, Thermo Fisher). An A-base was then added to the blunt ends of each strand to prepare them for ligation to indexed adapters. Each adapter contained a T-base overhang to ligate the adapter to A-tailed fragmented DNA. Dual-index adapters were ligated to the fragments and size selection was performed with AMPureXP beads. After

heat-labile UDG enzyme (m0280, NEB) treatment of the U-labeled second-stranded DNAs, the ligated products were amplified by PCR. Finally, we performed 2×150bp paired-end sequencing (PE150) on the Illumina Novaseq™ 6000 sequence platform following the vendor's recommended protocol. The obtained reads were filtered by Cutadapt (https://cutadapt.readthedocs.io/en/stable/, version: cutadapt-1.9). Raw sequence data were submitted to the NCBI Gene Expression Omnibus (GEO) datasets with accession numbers < GEO accession >. Data were aligned to the reference human genome using the HISAT2 package (https://daehwankimLab.github.io/hisat2/, version: hisat2-2.0.4). Differential gene expression analysis was performed using DESeq2 software between the two groups. Genes with FDR<0.05, and absolute fold change>1.2 were considered differentially expressed genes. Differentially expressed genes were then subjected to KEGG pathway enrichment and PPI analyses with the Cytoscape plugin tool MCODE. We also performed Gene Set Enrichment Analysis (GSEA) using GSEA software (v4.1.0) and MSigDB to identify whether a set of genes in specific KEGG pathways showed significant differences between the two groups. Briefly, we input the gene expression matrix and ranked the genes using the Signal2Noise normalization method. Enrichment scores and p-values were calculated in default parameters. KEGG pathways meeting this condition with |NES|>1, NOM p-value<0.05, and FDR q-value<0.25 were considered to be different between the two groups.

Immunofluorescence Analysis

HUVECs, with or without SNTSC-ApoEVs stimulation, were fixed in 4% paraformaldehyde for 20 min, permeabilized for 3 min with 0.1% Triton-100, blocked with 5% bovine serum albumin, and incubated with rabbit anti-COL1A1 (Beyotime, China) antibody overnight at 4°C, followed by incubation with Alexa Fluor 488-conjugated AffiniPure Goat anti-rabbit IgG secondary antibody (Jackson ImmunoResearch, USA) at room temperature for 60 min. The nuclei were counterstained with DAPI (Biosharp, China). Images were acquired sequentially with Olympus FV1000 laser scanning confocal microscope (Japan).

Lentivirus Transduction

An shRNA construct against COL1A1 was generated by Genomeditech (China). The target sequence for shRNA is ATGGATTCCAGTTCGAGTATG. The cells were then transduced with lentiviruses (MOI=20) in the medium of SNTSCs for 16 h and selected with 8 μg/mL puromycin. Transfection efficiency was detected by Western blot at 48 h post-transfection. Then shCOL1A1-SNTSC-ApoEVs were isolated from shCOL1A1-SNTSCs and evaluated with assays mentioned above.

PI3K Inhibition

To investigate the role of PI3K signaling in endothelial behavior, HUVECs were pretreated with the PI3K inhibitor LY294002 (10 μM; CSNpharm, China) for 2 h.[30] Then the culture medium was exchanged for the different medium treatments as described above.

Western Blot

Total proteins of SNTSC-ApoEVs and cells were extracted using RIPA buffer (Biosharp, China) containing protease and phosphatase inhibitors (Beyotime, China). Equal amounts of protein samples were loaded and run on 4–12% Sure PAGE gels (GenScript, China) and later transferred to PVDF membranes (Millipore, USA). The membrane was blocked with 5% BSA for 1 h at room temperature and then incubated with primary antibody at 4°C overnight. After washing with PBS containing 0.1% Tween 20 (TBST), the membranes were incubated with secondary antibodies (Beyotime, China) at room temperature for 1 h and washed again with TBST. The blots were imaged with a Western-Light chemiluminescence detection system (Millipore, USA) and analyzed with ImageJ software. Primary antibodies were specific for Caspase-3, Cleaved Caspase-3, VEGFA, CD31, PI3K, AKT, p-AKT and β-actin (Cell Signaling Technology).

Statistical Analysis

All experiments for each group were performed in triplicates. GraphPad Prism 8 (GraphPad Software, USA) was used for statistical and graphical analyses. All data were presented as mean ± standard deviation. Comparisons between two groups were performed using Student's *t*-test or Student's *t*-test with Welch's correction. For multi-group comparisons,

one-way analysis of variance (ANOVA) was used, and post-hoc analysis using Tukey's test was applied when appropriate. Differences were considered statistically significant at $p < 0.05$.

Results

SNTSC-ApoEVs Show Representative Characteristics of ApoEVs

First, we characterized the SNTSCs used in this study. Flow cytometry analysis revealed high expression of CD44, CD73, CD90, and CD105 but low expression of CD34, CD45, and HLA-DR (less than 1%) in SNTSCs (Figure S1A). Alizarin red, oil red O and Alcian blue positive staining indicated that SNTSCs exhibited osteogenic, lipogenic, and chondrogenic differentiation potential (Figure S1B).

SNTSC-ApoEVs were isolated through a sequential centrifuge procedure after apoptosis induction with STS for 16 h (Figure 1A). The apoptotic responses were confirmed through altered cell morphology and positive TUNEL staining in SNTSCs (Figure 1B and C). To determine the essential characteristics of ApoEVs, we analyzed their morphology, size distribution, and presence of apoptosis-associated markers. Our findings revealed that SNTSC-ApoEVs typically displayed a double-membrane spherical structure (Figure 1D) and were composed of a homogenous population with diameters between 30 and 700 nm (Figure 1E). The expressions of the apoptosis-associated markers PtdSer and Cleaved Caspase-3 were confirmed by Annexin V staining (Figure 1F) and Western blot analysis (Figure 1G). These findings indicated the successful isolation of ApoEVs.

SNTSC-ApoEVs Promote the Proliferation, Migration, Tube Formation and VEGFA Expression of HUVECs in vitro

To investigate the efficiency of SNTSC-ApoEVs in angiogenesis (Figure 2A), we first verified whether HUVECs could engulf SNTSC-ApoEVs. After incubation with SNTSC-ApoEVs for 8 h, internalization of PKH26-stained particles,

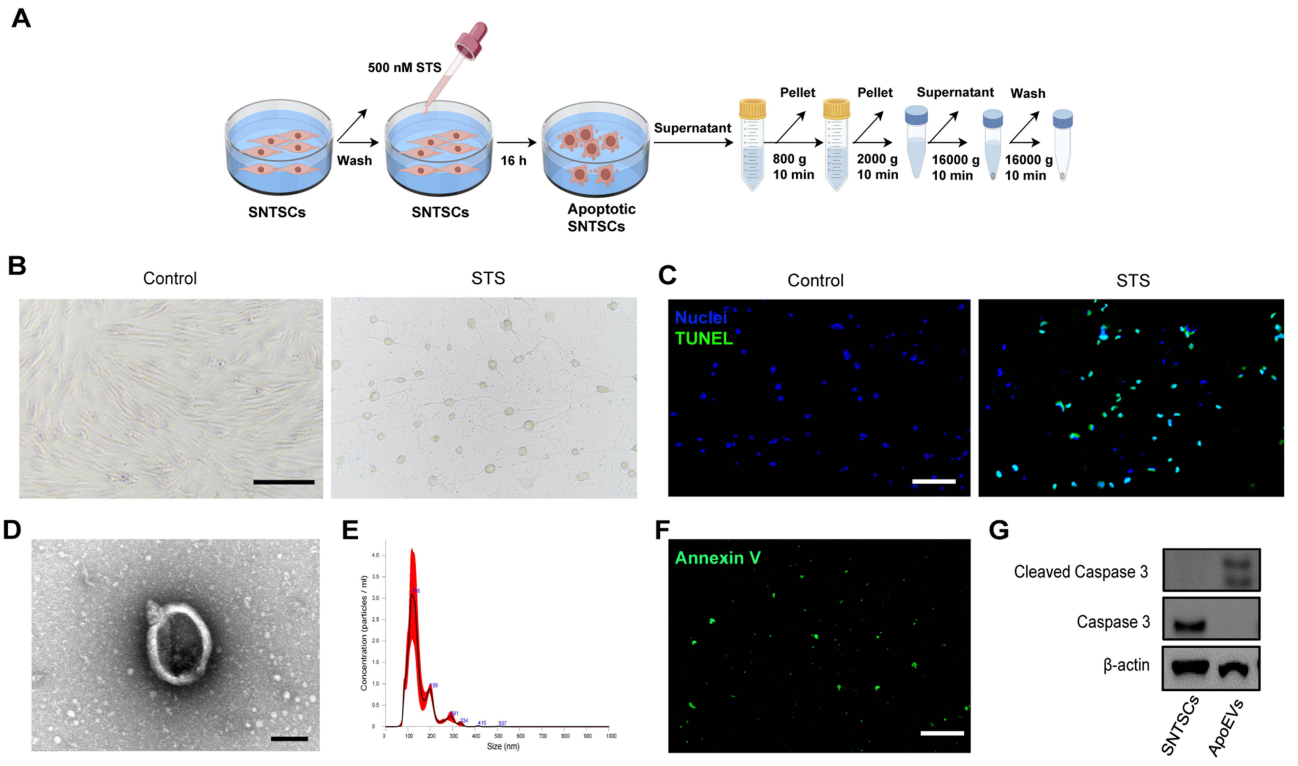

Figure 1 Characterization of SNTSC-derived ApoEVs. (**A**) Schematic drawing of the gradient centrifugation protocol for isolating ApoEVs from apoptotic SNTSCs. (**B**) Representative images of SNTSCs morphology before and after STS induction. (Scale bar=100 μm). (**C**) TUNEL analysis of apoptotic SNTSCs. (Scale bar=200 μm). (**D**) TEM image of SNTSC-ApoEVs. (Scale bar=100 nm). (**E**) NTA of SNTSC-ApoEVs shows the diameter and particle concentration. (**F**) Representative images of SNTSC-ApoEVs with Annexin V staining. (Scale bar=200 μm). (**G**) Western blot analysis of Cleaved Caspase-3 and Caspase-3 in SNTSCs and SNTSC-ApoEVs.

mainly in the cytoplasm, was confirmed by confocal microscopy (Figure 2B). Further tests were conducted to determine the effects of SNTSC-ApoEV concentrations (12.5, 25, 50, and 100 μg/mL) on HUVEC proliferation. CCK-8 analysis showed that 12.5 and 25 μg/mL SNTSC-ApoEVs significantly promoted HUVEC proliferation during the 3-day co-culture period, whereas doses over 50 μg/mL suppressed it (Figure 2C). Morphological changes in HUVECs were observed at doses over 50 μg/mL under a digital microscope (Figure S2). Therefore, 12.5 and 25 μg/mL were chosen for further investigation.

Increased endothelial migration behavior and tube formation capacity are typically associated with angiogenesis.[31] Scratch wound healing and transwell migration assays showed a significant increase in the closure percentage and number of migrated HUVECs in the 25 μg/mL SNTSC-ApoEVs group compared to the control and 12.5 μg/mL group (Figure 2D and E). The tube formation assay also confirmed that HUVECs organized into more intensive and extended capillary-like structures on Matrigel after induced with 25 μg/mL SNTSC-ApoEVs (Figure 2D and F).

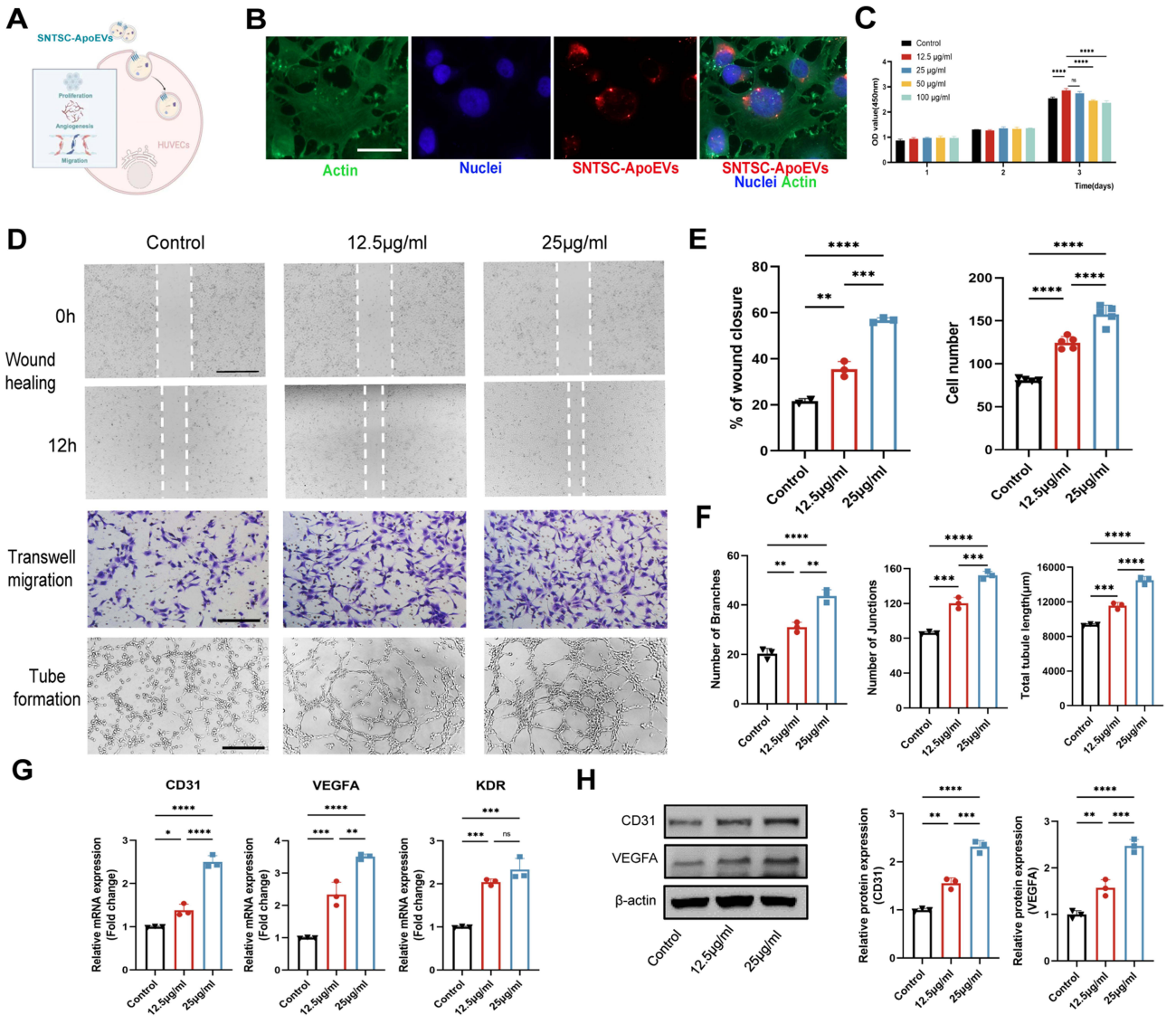

Figure 2 SNTSC-ApoEVs enhance the angiogenic capacity of HUVECs in vitro. (**A**) Experimental scheme for (**B-H**). (**B**) Uptake analysis of SNTSC-ApoEVs by HUVECs with laser scanning confocal microscopy (Red: DiR-labeled SNTSCs, green: cytoskeleton, blue: nucleus. Scare bar=50 μm). (**C**)The CCK-8 assay of HUVECs preincubated with culture medium supplemented with different concentration of SNTSC-ApoEVs in the 3-day period. (**D**) The images of migration and tube formation assays of HUVECs induced by 0, 12.5 and 25 μg/mL SNTSC-ApoEVs. (Scale bar=200 μm). (**E**) Quantitative analysis of closure percentage and cell migration among the three groups. (**F**) Quantitative analysis of tube formation among the three groups. (**G**) qRT-PCR analysis of effects of different concentrations of SNTSC-ApoEVs on the angiogenesis of HUVECs. (**H**) Western blot assays of CD31 and VEGFA in HUVECs under different doses of SNTSC-ApoEVs treatment. (^{ns}p >0.05, *p <0.05, **p <0.01, ***p<0.005, ****p<0.001).

Furthermore, qRT-PCR and Western blot revealed the highest proangiogenic gene and protein expression levels after 25 μg/mL SNTSC-ApoEVs treatment (Figure 2G and H), making it the optimal concentration. Notably, VEGFA stood out as the most differentially expressed proangiogenic gene. These data indicated that SNTSC-ApoEVs could promote the endothelial proliferation, migration, tube formation and upregulate VEGFA expression of HUVECs in vitro.

SNTSC-ApoEVs Facilitate Micro-Vessel Formation in vivo

To evaluate the effects of SNTSC-ApoEVs on blood vessel formation in vivo, we performed a Matrigel plug assay in mice (Figure 3A). After 7 days, all mice showed normal liver and kidney indices (Table S2), indicating the biosafety of SNTSC-ApoEVs. The proangiogenic properties of SNTSC-ApoEVs were assessed by CD31 labeled micro-vessel density. We detected more positively stained luminal structures in the SNTSC-ApoEVs group on day 7, and these micro-vessels presented a clearer pattern under higher magnification, as revealed by immunofluorescence assays (Figure 3B and C). These data demonstrated the potent promotional effect of SNTSC-ApoEVs on neovascularization in vivo.

COL1A1 is the Hub Extracellular Matrix-Cell Interaction-Related Protein in SNTSC-ApoEVs

Extracellular vesicles regulate receptor cell function through transferring proteins, lipids, and nucleic acids.[32] Therefore, we identified the proteomic compositions of SNTSC-ApoEVs with LC-MS/MS analysis. A total of 754 enriched proteins were identified in all samples.

Our proteomic analysis revealed that SNTSC-ApoEVs contained three categories of necessary proteins and one category of surface-binding proteins, which aligned with the requirements for extracellular vesicles components in the Minimal information for studies of extracellular vesicles 2018 (MISEV2018) guideline.[33] Among these, CD molecules, MHC class I, and integrin family were detected in Category 1 transmembrane or GPI-anchored proteins; Rho family, Annexin family, HSP family, and caveolin family were detected in Category 2 cytosolic proteins; lipoproteins, albumin,

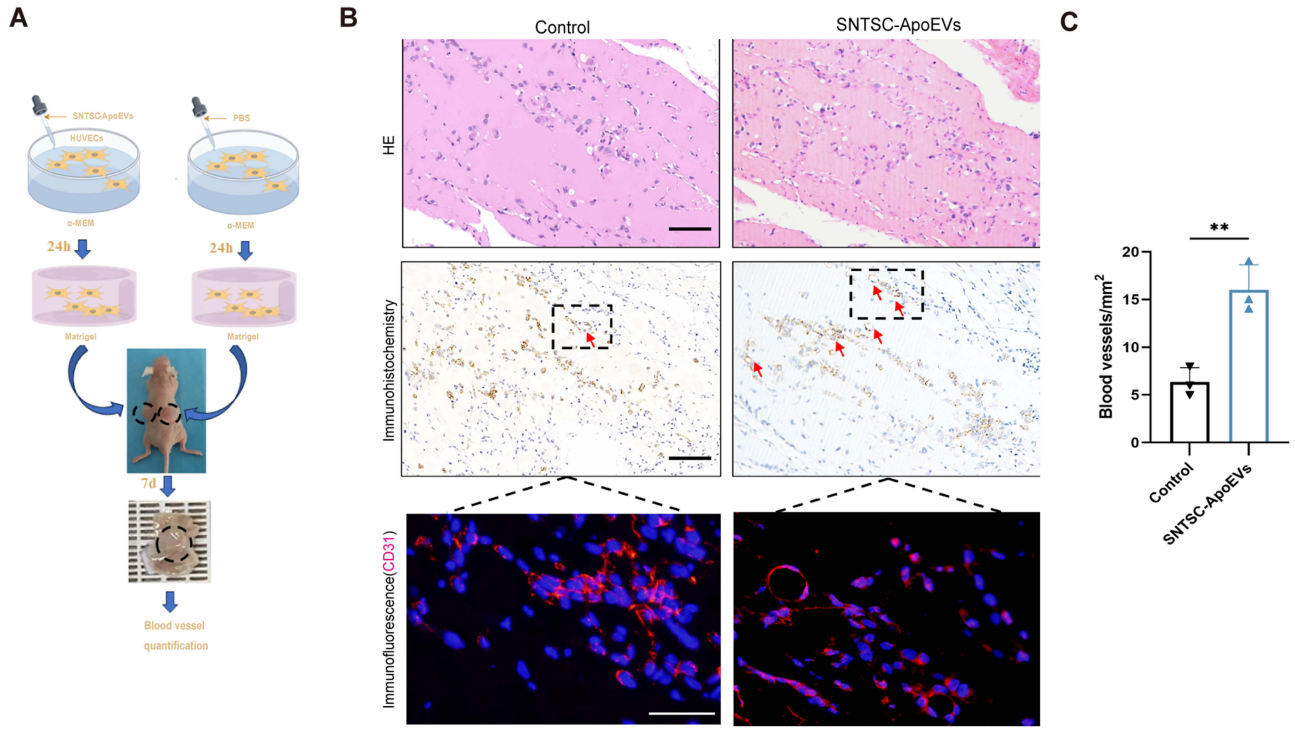

Figure 3 SNTSC-ApoEVs enhance vascularization in vivo. (**A**) Experimental scheme for (**B** and **C**). (**B**) Upper: Representative images of Matrigel plug at day 7 with H&E staining; Middle: Representative images of Matrigel plug at day 7 with immunohistochemical staining of CD31. The red arrows point out the blood vessels; Lower: Representative images of Matrigel plug at day 7 with immunofluorescence staining of CD31 under 200 magnified visual field. Red: CD31-stained blood vessels, blue: DAPI-stained nuclei. (Scale bars=100 μm). (**C**) Quantitative analysis of blood vessel numbers per 50 magnified visual field in immunohistochemistry at day 7 (**p <0.01).

and several ribosomal proteins were detected in Category 3 co-isolated non-vesicular structured proteins. Moreover, various cytokines and growth factors were detected in Category 5 secretory proteins and extracellular matrix proteins, whereas no proangiogenic cytokines or growth factors were found. Additionally, apoptotic markers, including Fas, Sod1, and Caspase family, were identified.

Further GO enrichment functional analysis showed that the enriched proteins were derived from extracellular vesicles, adherens junction, cell-substrate junction, and focal adhesion (Figure 4A), suggesting that these proteins are mainly associated with vesicle and cell-substrate interactions. Enrichment analysis of biological process showed that the enriched proteins may play key roles in collagen metabolic process, cell adhesion, extracellular matrix organization, and focal adhesion assembly (Figure 4B). Enrichment analysis of molecular function revealed that the enriched proteins contributed to the regulation of metabolic processes, including cell adhesion molecule binding, oxidoreductase activity, and nucleoside-triphosphatase activity (Figure 4C). Moreover, KEGG pathway analysis revealed that enriched proteins were associated with "Regulation of actin cytoskeleton", "Focal adhesion", "ECM-receptor interaction", and "PI3K-Akt signaling pathway" (Figure 4D). These findings suggested a potential role of SNTSC-ApoEV functional proteins in regulating extracellular matrix-cell interactions in HUVECs.

Therefore, we further performed PPI network analysis on the enriched proteins in the pathways including "Regulation of actin cytoskeleton", "Focal adhesion", "ECM-receptor interaction", and "PI3K-Akt signaling pathway", and obtained the top 10 hub proteins, which are listed in order as follows: COL1A1, COL1A2, FN1, COL3A1, ACTB, ITGB1, GAPDH, ALB, CD44 and ITGAV (Figure 4E). Notably, COL1A1, a crucial component of the extracellular matrix, was

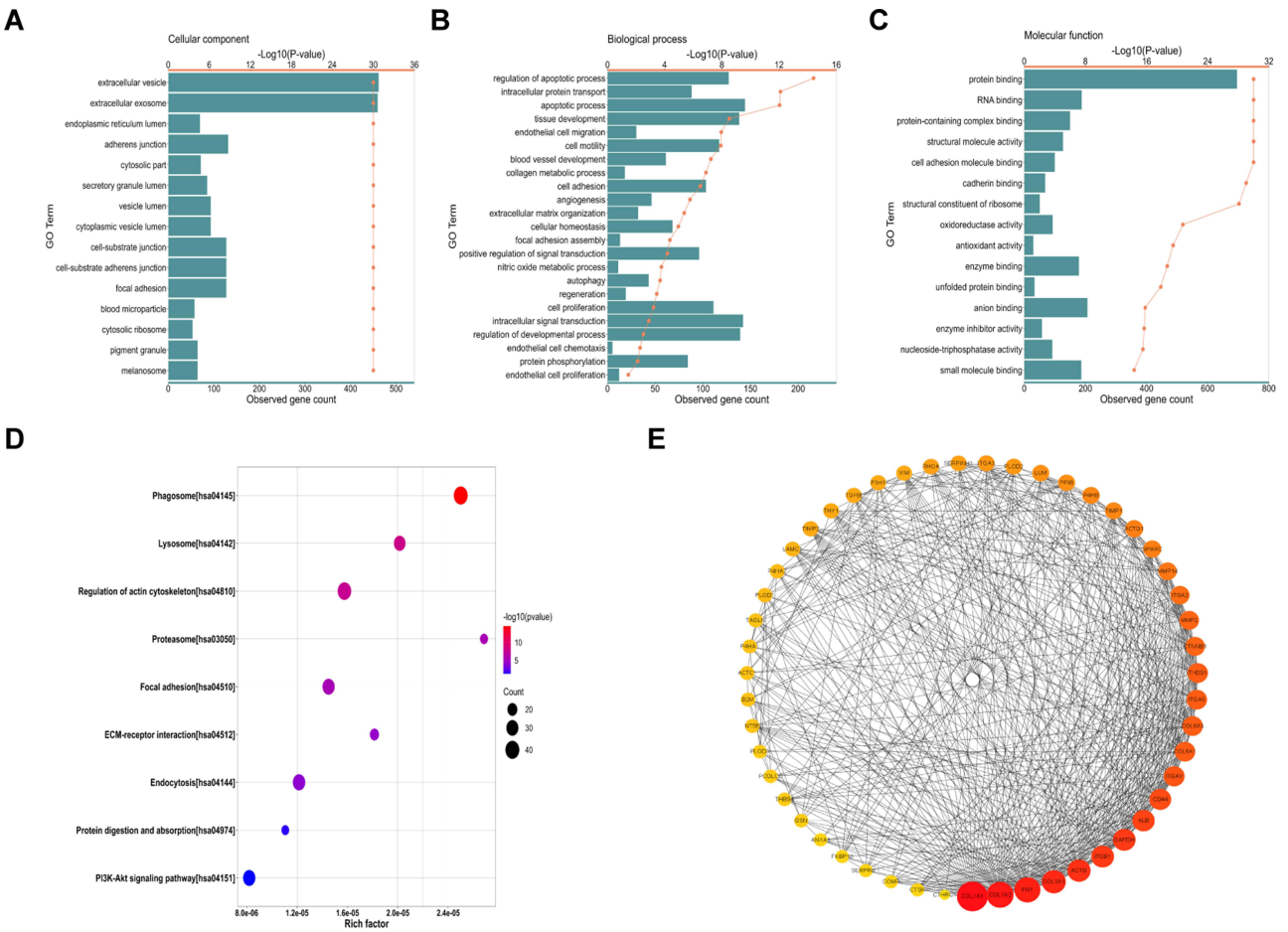

Figure 4 Proteomic profile of SNTSC-ApoEVs. (**A**) GO enrichment analysis of cellular compartments. (**B**) GO enrichment analysis of biological process. (**C**) GO enrichment analysis of molecular function. (**D**) KEGG pathway analysis of enriched proteins. (**E**) PPI analysis of enriched proteins in pathways associated with extracellular matrix-cell interactions.

found to be the hub protein with the highest connectivity, indicating its potential as a vital target protein for signal transduction from SNTSC-ApoEVs to HUVECs.[34]

SNTSC-ApoEVs Transfer COL1A1 to Regulate HUVEC Function by Activating the PI3K/Akt/VEGF Pathway

To elucidate the detailed signaling pathways related to the proangiogenic role of SNTSC-ApoEVs, RNA-seq analysis of SNTSC-ApoEVs-treated and control HUVECs was performed. In total, 5863 genes were found to be differentially expressed, including 3766 upregulated and 2097 downregulated genes (Figure S3A and B). KEGG pathway analysis showed that differentially expressed genes (DEGs) was related to multiple signal transductions (Figure 5A), and GSEA also revealed enrichment patterns of gene signatures involved in "PI3K-AKT signaling pathway", "cell cycle", and "inositol phosphate metabolism" (Figures 5B and S3C). Among these, the PI3K/AKT signaling pathway was the most abundant.

Next, we generated a MCODE key subnetwork of all DEGs in the PI3K/AKT pathway and found that COL1A1 was the hub gene with the highest connectivity (Figure 5C). Therefore, we performed qRT-PCR and immunofluorescence analyses. The results demonstrated an elevation in the mRNA and protein expression levels of COL1A1 in HUVECs after stimulation with SNTSC-ApoEVs (Figure 5D and E). These findings suggested that COL1A1 and PI3K/Akt pathway may play crucial roles as downstream signaling molecule and pathway in angiogenesis of HUVECs under SNTSC-ApoEVs treatment.

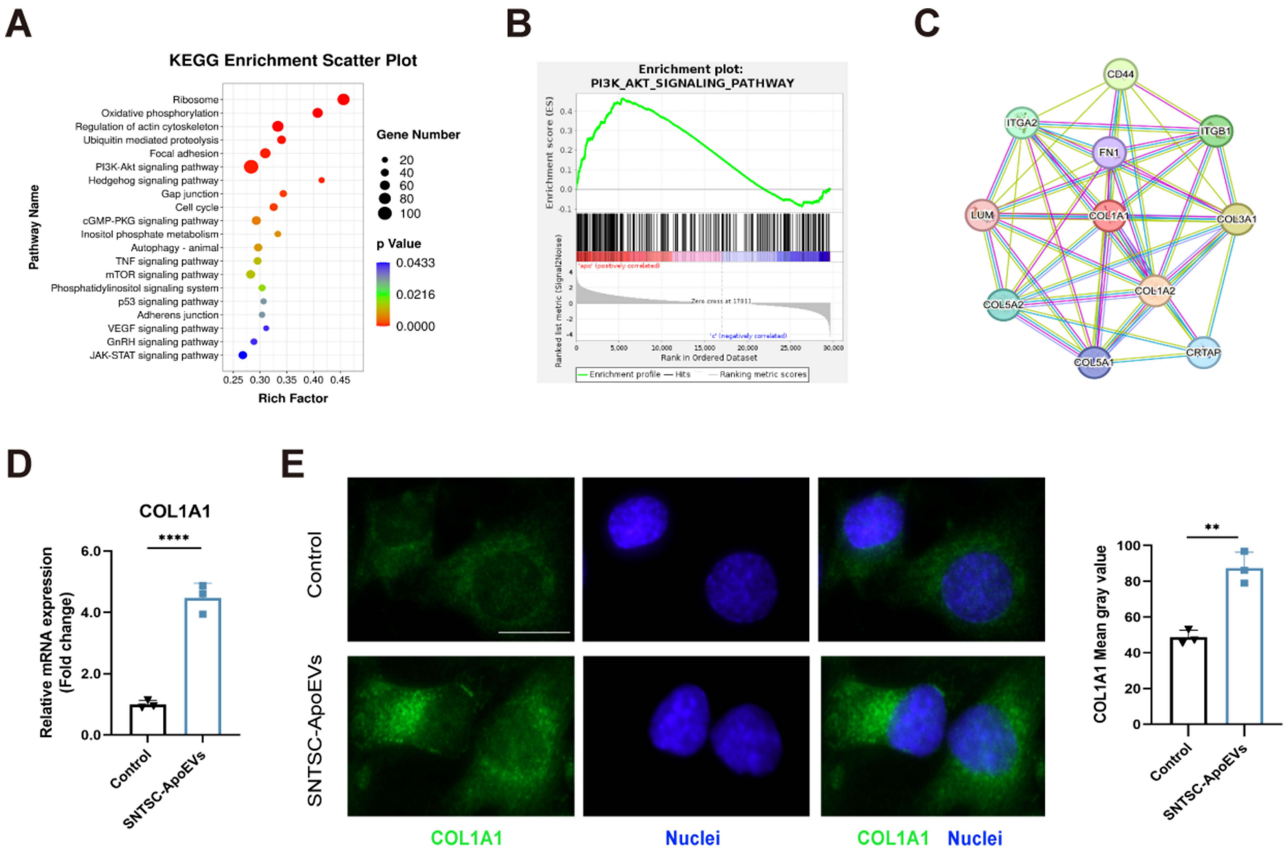

Figure 5 SNTSC-ApoEVs modulate PI3K/Akt pathway and COL1A1 expression in HUVECs. (**A**) KEGG pathway analysis of significantly upregulated genes in HUVECs treated with SNTSC-ApoEVs. (**B**) GSEA shows the enrichment patterns of gene signatures involved in "PI3K-AKT signaling pathway". (**C**) Hub genes based on PPI analysis of DEGs in the PI3K-AKT signaling pathway. (**D**) qRT-PCR analysis of SNTSC-ApoEV effect on COL1A1 mRNA expression. (**E**) Representative immunofluorescent images of HUVECs under SNTSC-ApoEVs treatment (Green: COL1A1 protein, blue: nucleus. Scare bar=20 μm.) and quantitative analysis of COL1A1 mean gray value. (**p <0.01, ****p<0.001).

To further explore whether COL1A1 targeted PI3K/Akt signaling to regulate endothelial functions, we used shRNA to knock down COL1A1 expression in SNTSCs and subsequently generated ApoEVs (Figure 6A). After confirming the efficiency of COL1A1 shRNA knockdown in SNTSC-ApoEVs by Western blot analysis (Figure 6B), we found that shCOL1A1-SNTSC-ApoEVs failed to upregulate the expression of COL1A1 in HUVECs (Figure 6C), indicating that increased COL1A1 expression in HUVECs was caused by direct transport from SNTSC-ApoEVs. The protein levels of PI3K and VEGFA and the p-AKT/AKT ratio in the shCOL1A1-SNTSC-ApoEVs group were also lower than those in the SNTSC-ApoEVs group (Figure 6C), suggesting that PI3K/Akt/VEGF pathway signals of HUVECs were downregulated after COL1A1 inhibition in SNTSC-ApoEVs. Additionally, shCOL1A1-SNTSC-ApoEVs possessed a reduced capacity to enhance endothelial proliferation, migration, tube formation in vitro (Figure 6D-G), and exhibited a decreased capacity to promote micro-vessel formation in vivo compared to the SNTSC-ApoEVs group (Figure 6H and I). These data suggested that SNTSC-ApoEVs transferred COL1A1 to target the PI3K/Akt/VEGF pathway and energize HUVECs angiogenic functions.

Moreover, to determine the involvement of the PI3K/Akt pathway in the proangiogenic effects induced by SNTSC-ApoEVs, HUVECs were pretreated with 10 μM PI3K inhibitor LY294002 (Figure 7A). A decrease in the p-AKT/AKT ratio was observed in the LY group compared to the control group, indicating the effectiveness of the inhibitor (Figure 7B). In the SNTSC-ApoEVs + LY group, LY294002 significantly antagonized the enhancing effects of SNTSC-ApoEVs on the protein level of PI3K and p-AKT/AKT ratio (Figure 7B), reversed the increase in endothelial cell proliferation (Figure 7C), suppressed the migration capacity (Figure 7D and E), downregulated the organization of HUVECs into capillary-like structures on Matrigel (Figure 7D and F), and partly blocked the upregulation in VEGFA protein levels in vitro (Figure 7G). Cumulatively, these evidence indicated that SNTSC-ApoEVs promoted revascularization via the transfer of COL1A1 and the activation of the PI3K/Akt/VEGF pathway (Figure 8).

Discussion

Angiogenesis is a prerequisite for tissue repair and regeneration, and crucial for the treatment of ischemic diseases including myocardial infarction, diabetic microangiopathy, limb ischemia, pulp necrosis.[2,12,20,35] Intriguingly, accumulating evidence has proven that ApoEVs from apoptotic MSCs play an indispensable role in accelerating this progress.[36] To avoid sampling problems of previously used MSCs, STNSCs have emerged as a compelling alternative source of ApoEVs, as they are more easily accessible and can be harvested non-invasively.[37] SNTSCs were chosen over permanent dental pulp stem cells (DPSCs) owing to stronger proliferative capacity and higher expression levels of multiple proliferation-related genes, which is beneficial for ApoEVs mass production.[25] However, the detailed features of ApoEVs from SNTSCs remain incompletely understood.

In this study, we investigated the morphology, size, proangiogenic capacity, and protein profiles of SNTSC-ApoEVs, along with transcriptional changes in HUVECs after SNTSC-ApoEVs stimulation. We demonstrated that SNTSC-ApoEVs enhanced angiogenesis of HUVECs in vitro and promoted micro-vessel formation in a Matrigel plug model in vivo. In addition to expressing general ApoEVs markers, SNTSC-ApoEVs were enriched with multiple proteins related to extracellular matrix-cell interactions. Mechanistically, SNTSC-ApoEVs transferred COL1A1 to HUVECs and promoted endothelial cell function by activating the PI3K/Akt/VEGF cascade.

TEM and NTA results revealed that the isolated SNTSC-ApoEVs exhibited a typical morphology, with less than 1 μm in diameter. ApoEVs with smaller diameters (< 1 μm) have been reported to have superior membrane integrity for molecular exchange over apoptotic bodies (> 1 μm),[16] which boosts our confidence in subsequent experiments and potential clinical translation.

HUVECs were chosen as the recipient cells due to their status as one of the major effector cells during neovascularization.[38] The stimulation duration was set to 24 h to ensure that the observed effects were mainly caused by the transported miRNAs or proteins.[35,39] SNTSC-ApoEVs isolated in this study showed the highest proliferation stimulation effect at a concentration of 25 μg/mL. This optimal concentration is similar to previous results ofstudies on ApoEVs from human deciduous pulp stem cells and exosomes released by DPSCs.[20,39–41] Furthermore, we used the Matrigel plug assay to investigate the micro-vessel formation capacity of SNTSC-ApoEVs as previously reports on

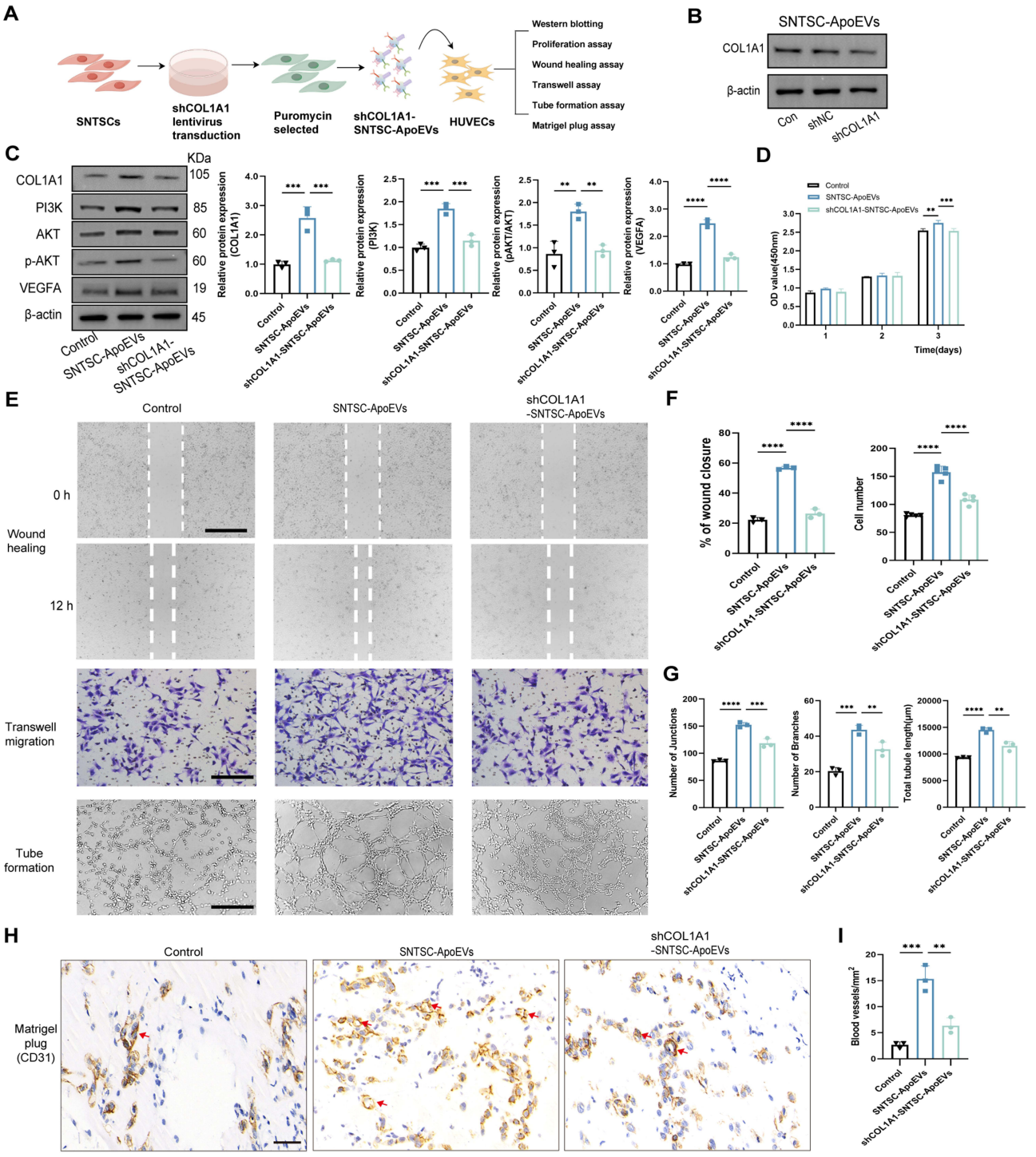

Figure 6 COL1A1 downregulation in SNTSC-ApoEVs inhibits the COL1A1/PI3K/Akt/VEGF cascades of HUVECs and reduces the endothelial function. (**A**) Experimental scheme for (**B-I**). (**B**) Representative Western blot images of COL1A1 protein expression in ApoEVs released from shNC- or shCOL1A1-transduced SNTSCs. (**C**) Representative Western blot images and quantitative analysis of COL1A1, PI3K, AKT, p-AKT and VEGFA protein expression in HUVECs after SNTSC-ApoEVs or shCOL1A1-SNTSC-ApoEVs stimulation. (**D**) Cell viability of HUVECs after SNTSC-ApoEVs or shCOL1A1-SNTSC-ApoEVs stimulation detected by CCK-8 assays at days 1, 2 and 3. (**E**) Representative images of migration and tube formation assays in HUVECs induced by SNTSC-ApoEVs or shCOL1A1-SNTSC-ApoEVs. (Scale bar= 200 μm). (**F**) Quantitative analysis of closure percentage and cell migration among the three groups. (**G**) Quantitative analysis of tube formation among the three groups. (**H**) Representative immunohistochemical staining images of Matrigel plug treated with SNTSC-ApoEVs or shCOL1A1-SNTSC-ApoEVs at day 7. The red arrows point out the CD31-stained blood vessels. (Scale bar= 50 μm). (**I**) Quantitative analysis of blood vessel numbers per 50 magnified visual field in immunohistochemistry at day 7. (**p <0.01, ***p<0.005, ****p<0.001).

https://doi.org/10.2147/IJN.S466136 DovePress

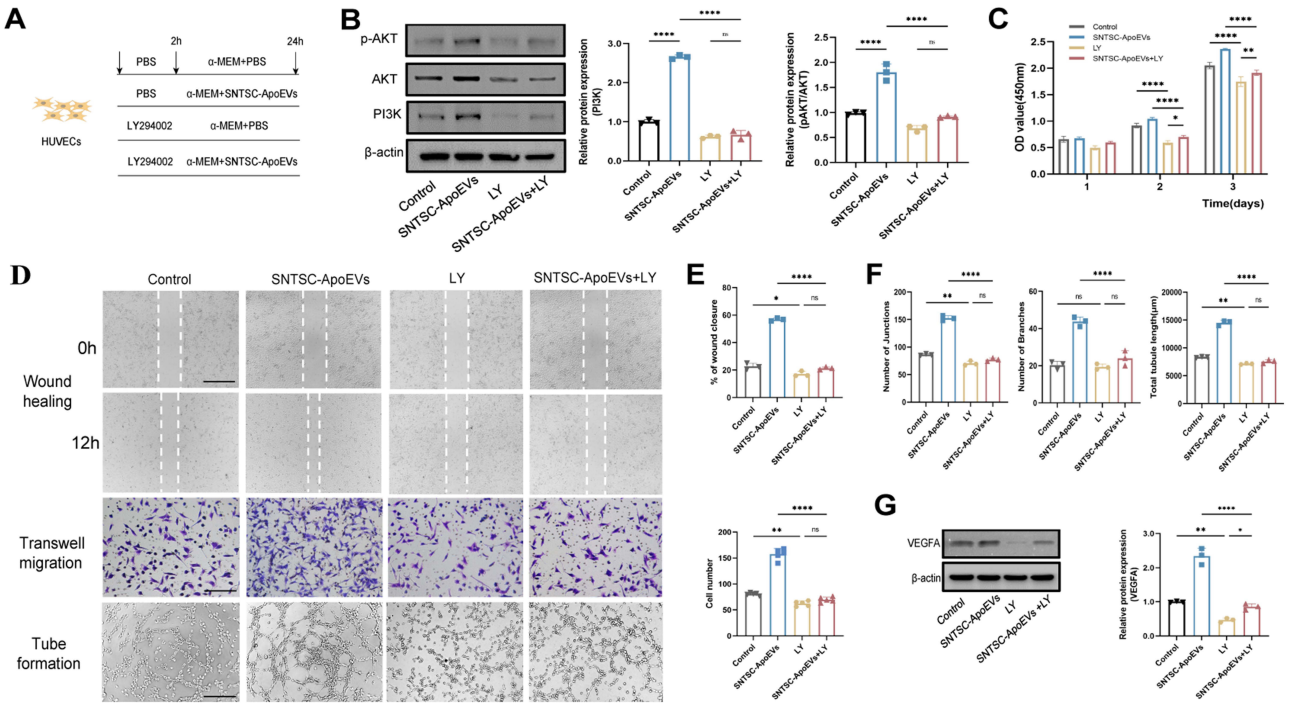

Figure 7 Proangiogenic capacity of SNTSC-ApoEVs in HUVECs is attenuated when PI3K/AKT pathway is blocked. (**A**) Experimental scheme for (**B-G**). (**B**) Representative Western blot images (left) and quantitative analysis (right) of PI3K, AKT, and p-AKT protein expression in HUVECs treated with medium supplemented with control, SNTSC-ApoEVs, LY294002 and SNTSC-ApoEVs+LY294002. (LY: LY294002). (**C**) Cell proliferation of HUVECs in four groups detected by CCK-8 assays at days 1, 2, and 3. (**D**) Representative images of cell migration and tube formation assays under different induction. (Scale bar= 200 μm). (**E** and **F**) Quantitative analysis of cell migration and tube formation ability. (**G**) Representative Western blot images and quantitative analysis of VEGFA protein expression in HUVECs under different treatment. (^{ns}p >0.05, $^{*}p$ <0.05, $^{**}p$ <0.01, $^{****}p$<0.001).

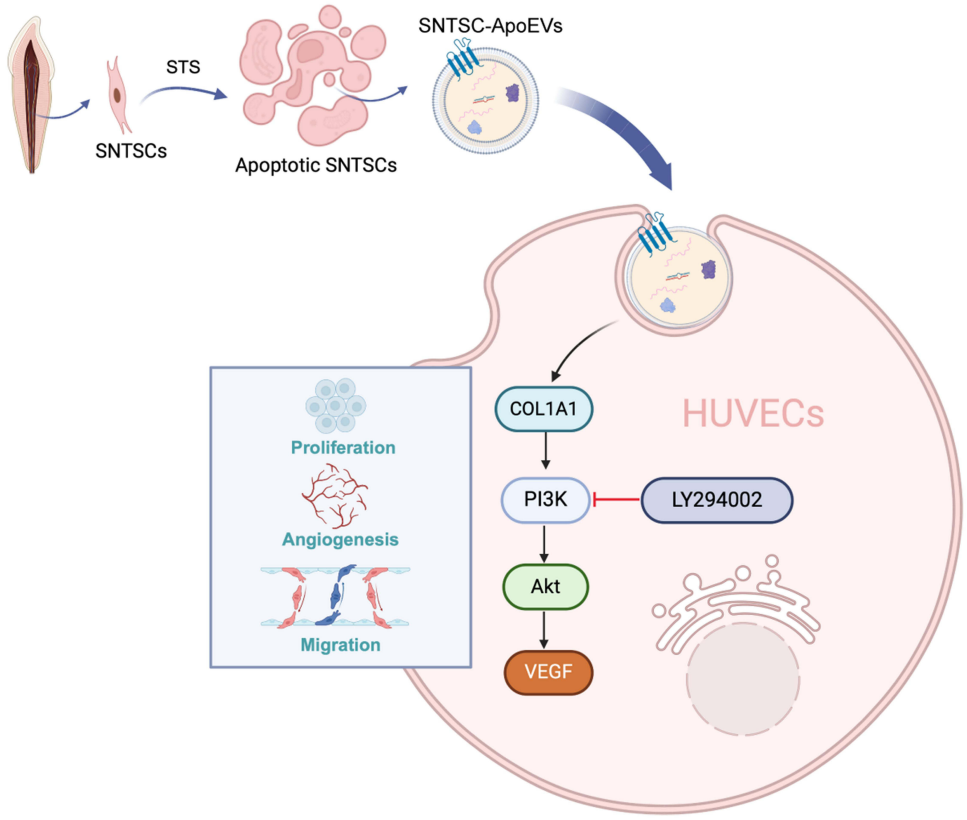

Figure 8 SNTSC-ApoEVs promote angiogenesis by transferring function molecule COL1A1 and activating PI3K/Akt/VEGF pathway.

extracellular vesicles described.[42,43] Quantification of the newly formed vessel marker CD31 staining[44] showed SNTSC-ApoEVs successfully developed more micro-vessels in vivo.

From the perspective of clinical transformation, it is necessary to determine the active ingredients and proangiogenic mechanism of ApoEVs, which is important in controlling the efficacy and safety of ApoEVs-based therapy.[3] Through proteomic analysis, we detected the 13 proteins enriched in ApoEVs from human BMMSCs and ADMSCs in SNTSC-ApoEVs. This discovery lends support to the hypothesis that MSC-derived ApoEVs exhibit overlapping proteomic profiles.[10] Further functional analysis revealed that multiple proteins were associated with extracellular matrix-cell interactions, and COL1A1 was identified as the hub protein based on PPI analysis. Moreover, we analyzed the transcriptional profile of HUVECs and found that COL1A1 was significantly upregulated under SNTSC-ApoEVs stimulation. COL1A1, an α1 chain of type I collagen, is a secreted proteins associated with extracellular vesicles,[33] and plays an essential role in specific interactions between cell surface and transmembrane molecules.[45,46] Previous studies have shown that COL1A1 is associated with cell migration and proliferation capacity in inadequate angiogenesis-related diseases, including cardiovascular diseases and diabetic retinopathy.[47,48] Here, we knocked down COL1A1 in SNTSCs to downregulate COL1A1 expression in ApoEVs, and found that SNTSC-ApoEVs-derived COL1A1 was responsible for the proangiogenic role of SNTSC-ApoEVs by promoting the expression of VEGFA, enhancing endothelial cell functions and facilitating micro-vessels formation. Given that our proteomic analysis did not detect VEGF or other proangiogenic factors in SNTSC-ApoEVs, direct transport was ruled out as the cause of the upregulated VEGFA expression in HUVECs.

The effect of COL1A1 on VEGFA expression was further investigated, and KEGG analysis revealed that the PI3K/Akt pathway played a crucial role in SNTSC-ApoEVs-induced endothelial function. Studies have shown that activation of the PI3K/Akt signaling pathway is closely associated with endothelial proliferation, migration, and tube formation.[49,50] According to our data, the PI3K/Akt/VEGF pathway was activated by SNTSC-ApoEVs-derived COL1A1, and PI3K inhibition significantly reduced the stimulatory effects of SNTSC-ApoEVs on the proliferation, migration, and tube formation capacity of HUVECs.

Notably, the partial reversal effect induced by the PI3K inhibitor on proliferation and VEGFA expression suggests the involvement of multiple pathways in this angiogenic process. In reference to the proangiogenic mechanisms of ApoEVs from human deciduous pulp stem cells and rat BMMSCs,[12,20] although we did not detect the enrichment of autophagy-related pathways in SNTSC-ApoEVs by proteomic functional analysis, activation of AKT in HUVECs was also observed under SNTSC-ApoEVs treatment in this study, further indicating the possibility of multiple pathway interactions. Our findings highlight the need for further research to fully understand the mechanisms underlying the effects of SNTSC-ApoEVs on angiogenesis.

Conclusion

In conclusion, our study is the first to show that COL1A1 transferred from SNTSC-ApoEVs plays a role in modulating the PI3K/Akt/VEGF signaling pathway, thereby enhancing endothelial cell function. These findings deepen our understanding of ApoEVs-induced neovascularization mechanisms and highlight the potential of ApoEVs as therapeutic options for angiogenesis-related disorders.

Abbreviations

ADMSCs: Adipose-derived mesenchymal stem cell; ApoEVs: Apoptotic extracellular vesicles; BMMSCs: Bone marrow mesenchymal stem cell; DEGs: Differentially expressed genes; DPSCs: Dental pulp stem cells; FAK: Focal Adhesion Kinase; GO: Gene ontology; GSEA: Gene set enrichment analysis; H&E: Hematoxylin and eosin; HUVECs: Human umbilical vein endothelial cells; KEGG: Kyoto Encyclopedia of Genes and Genomes; KDR: Kinase insert domain receptor; MSCs: Mesenchymal stem cells; NTA: Nanoparticle tracking analysis; PI3K: Phosphatidylinositol-4,5-bisphosphate 3-kinase; PtdSer: Phosphatidylserine; RNA-Seq: RNA Sequencing; SNTSCs: Supernumerary tooth-derived pulp stem cells; SNTSC-ApoEVs: Apoptotic extracellular vesicles from supernumerary tooth-derived pulp stem cells; STS: Staurosporine; TBST: PBS containing 0.1% Tween 20; TEM: Transmission Electron Microscope; TUNEL: Terminal deoxynucleotidyl transferase-mediated dUTP nick end labeling; VEGFA: Vascular endothelial growth factor A.

Data Sharing Statement

The datasets used and/or analyzed during the current study are available from the corresponding author upon reasonable request.

Acknowledgments

The authors appreciate the help of Dr. Huiwen Chen for excellent schematic drawing, Dr. Guangyun Lai, Dr. Yuancheng Lv, Dr. Xueqin Zhu and Dr. Zhangke Ma for their constructive comments during the review process.

Author Contributions

All authors made a significant contribution to the work reported, whether that is in the conception, study design, execution, acquisition of data, analysis and interpretation, or in all these areas; took part in drafting, revising or critically reviewing the article; gave final approval of the version to be published; have agreed on the journal to which the article has been submitted; and agree to be accountable for all aspects of the work.

Funding

The authors disclosed receipt of the following financial support for the research, authorship, and/or publication of this article: This work was supported by the Natural Science Foundation of Shanghai (23ZR1437800), Biomaterials and Regenerative Medicine Institute Cooperative Research Project, Shanghai Jiaotong University School of Medicine (2022LHB06), and Biological Clinical Sample Project of Shanghai Ninth People's Hospital (YBKB202222).

Disclosure

The authors report no conflicts of interest in this work.

References

1. Todorova D, Simoncini S, Lacroix R, Sabatier F, Dignat-George F. Extracellular Vesicles in Angiogenesis. *Circ Res*. 2017;120(10):1658–1673. doi:10.1161/CIRCRESAHA.117.309681
2. Eelen G, Treps L, Li X, Carmeliet P. Basic and Therapeutic Aspects of Angiogenesis Updated. *Circ Res*. 2020;127(2):310–329. doi:10.1161/circresaha.120.316851
3. Pan Z, Sun W, Chen Y, et al. Extracellular Vesicles in Tissue Engineering: biology and Engineered Strategy. *Adv Healthc Mater*. 2022;11(21):e2201384. doi:10.1002/adhm.202201384
4. Chen Y, Huang J, Chen R, et al. Sustained release of dermal papilla-derived extracellular vesicles from injectable microgel promotes hair growth. *Theranostics*. 2020;10(3):1454–1478. doi:10.7150/thno.39566
5. Lin R, Zhang T, Gao J. Apoptotic Vesicles of MSCs: the Natural Therapeutic Agents and Bio-Vehicles for Targeting Drug Delivery. *Small*. 2023;19:e2301671. doi:10.1002/smLl.202301671
6. Zheng C, Sui B, Zhang X, et al. Apoptotic vesicles restore liver macrophage homeostasis to counteract type 2 diabetes. *J Extracell Vesicles*. 2021;10(7):e12109. doi:10.1002/jev2.12109
7. Gregory CD, Dransfield I. Apoptotic Tumor Cell-Derived Extracellular Vesicles as Important Regulators of the Onco-Regenerative Niche. *Front Immunol*. 2018;9:1111. doi:10.3389/fimmu.2018.01111
8. Zhu Y, Chen X, Liao Y. Mesenchymal Stem Cells-Derived Apoptotic Extracellular Vesicles (ApoEVs): mechanism and Application in Tissue Regeneration. *Stem Cells*. 2023;41(9):837–849. doi:10.1093/stmcls/sxad046
9. Zou X, Lei Q, Luo X, et al. Advances in biological functions and applications of apoptotic vesicles. *Cell Commun Signal*. 2023;21(1):260. doi:10.1186/s12964-023-01251-9
10. Zhang X, Tang J, Kou X, et al. Proteomic analysis of MSC-derived apoptotic vesicles identifies Fas inheritance to ameliorate haemophilia a via activating platelet functions. *J Extracell Vesicles*. 2022;11(7):e12240. doi:10.1002/jev2.12240
11. Xin L, Wei C, Tong X, et al. In situ delivery of apoptotic bodies derived from mesenchymal stem cells via a hyaluronic acid hydrogel: a therapy for intrauterine adhesions. *Bioact Mater*. 2022;12:107–119. doi:10.1016/j.bioactmat.2021.10.025
12. Liu H, Liu S, Qiu X, et al. Donor MSCs release apoptotic bodies to improve myocardial infarction via autophagy regulation in recipient cells. *Autophagy*. 2020;16(12):2140–2155. doi:10.1080/15548627.2020.1717128
13. Grant LR, Milic I, Devitt A. Apoptotic cell-derived extracellular vesicles: structure-function relationships. *Biochem Soc Trans*. 2019;47(2):509–516. doi:10.1042/bst20180080
14. Ma L, Chen C, Liu D, et al. Apoptotic extracellular vesicles are metabolized regulators nurturing the skin and hair. *Bioact Mater*. 2023;19:626–641. doi:10.1016/j.bioactmat.2022.04.022
15. Qu Y, He Y, Meng B, et al. Apoptotic vesicles inherit SOX2 from pluripotent stem cells to accelerate wound healing by energizing mesenchymal stem cells. *Acta Biomater*. 2022;149:258–272. doi:10.1016/j.actbio.2022.07.009
16. Kakarla R, Hur J, Kim YJ, Kim J, Chwae YJ. Apoptotic cell-derived exosomes: messages from dying cells. *Exp Mol Med*. 2020;52(1):1–6. doi:10.1038/s12276-019-0362-8

17. Phan TK, Ozkocak DC, Poon IKH. Unleashing the therapeutic potential of apoptotic bodies. *Biochem Soc Trans*. 2020;48(5):2079–2088. doi:10.1042/BST20200225
18. Wang R, Hao M, Kou X, et al. Apoptotic vesicles ameliorate lupus and arthritis via phosphatidylserine-mediated modulation of T cell receptor signaling. *Bioact Mater*. 2023;25:472–484. doi:10.1016/j.bioactmat.2022.07.026
19. Fu Y, Sui B, Xiang L, et al. Emerging understanding of apoptosis in mediating mesenchymal stem cell therapy. *Cell Death Dis*. 2021;12(6):596. doi:10.1038/s41419-021-03883-6
20. Li Z, Wu M, Liu S, et al. Apoptotic vesicles activate autophagy in recipient cells to induce angiogenesis and dental pulp regeneration. *Mol Ther*. 2022;30(10):3193–3208. doi:10.1016/j.ymthe.2022.05.006
21. Li J, Wei C, Yang Y, Gao Z, Guo Z, Qi F. Apoptotic bodies extracted from adipose mesenchymal stem cells carry microRNA-21-5p to induce M2 polarization of macrophages and augment skin wound healing by targeting KLF6. *Burns*. 2022;48(8):1893–1908. doi:10.1016/j.burns.2021.12.010
22. Kerkis I, Kerkis A, Dozortsev D, et al. Isolation and characterization of a population of immature dental pulp stem cells expressing OCT-4 and other embryonic stem cell markers. *Cells Tissues Organs*. 2006;184(3–4):105–116. doi:10.1159/000099617
23. Bernardi L, Luisi SB, Fernandes R, et al. The isolation of stem cells from human deciduous teeth pulp is related to the physiological process of resorption. *J Endod*. 2011;37(7):973–979. doi:10.1016/j.joen.2011.04.010
24. Makino Y, Yamaza H, Akiyama K, et al. Immune therapeutic potential of stem cells from human supernumerary teeth. *J Dent Res*. 2013;92(7):609–615. doi:10.1177/0022034513490732
25. Lu X, Liu SF, Wang HH, et al. A biological study of supernumerary teeth derived dental pulp stem cells based on RNA-seq analysis. *Int Endod J*. 2019;52(6):819–828. doi:10.1111/iej.13060
26. Guerrero-Jiménez M, Nic-Can GI, Castro-Linares N, et al. In vitro histomorphometric comparison of dental pulp tissue in different teeth. *PeerJ*. 2019;7:e8212. doi:10.7717/peerj.8212
27. Yang H, Gao LN, An Y, et al. Comparison of mesenchymal stem cells derived from gingival tissue and periodontal ligament in different incubation conditions. *Biomaterials*. 2013;34(29):7033–7047. doi:10.1016/j.biomaterials.2013.05.025
28. Sun HH, Chen B, Zhu QL, et al. Investigation of dental pulp stem cells isolated from discarded human teeth extracted due to aggressive periodontitis. *Biomaterials*. 2014;35(35):9459–9472. doi:10.1016/j.biomaterials.2014.08.003
29. Ma Q, Liang M, Wu Y, et al. Osteoclast-derived apoptotic bodies couple bone resorption and formation in bone remodeling. *Bone Res*. 2021;9(1):5. doi:10.1038/s41413-020-00121-1
30. Deregibus MC, Cantaluppi V, Doublier S, et al. HIV-1-Tat protein activates phosphatidylinositol 3-kinase/ AKT-dependent survival pathways in Kaposi's sarcoma cells. *J Biol Chem*. 2002;277(28):25195–25202. doi:10.1074/jbc.M200921200
31. Migneault F, Dieudé M, Turgeon J, et al. Apoptotic exosome-like vesicles regulate endothelial gene expression, inflammatory signaling, and function through the NF-κB signaling pathway. *Sci Rep*. 2020;10(1):12562. doi:10.1038/s41598-020-69548-0
32. Liu D, Kou X, Chen C, et al. Circulating apoptotic bodies maintain mesenchymal stem cell homeostasis and ameliorate osteopenia via transferring multiple cellular factors. *Cell Res*. 2018;28(9):918–933. doi:10.1038/s41422-018-0070-2
33. Théry C, Witwer KW, Aikawa E, et al. Minimal information for studies of extracellular vesicles 2018 (MISEV2018): a position statement of the International Society for Extracellular Vesicles and update of the MISEV2014 guidelines. *J Extracell Vesicles*. 2018;7(1):1535750. doi:10.1080/20013078.2018.1535750
34. Wu SC, Kuo PJ, Rau CS, et al. Increased Angiogenesis by Exosomes Secreted by Adipose-Derived Stem Cells upon Lipopolysaccharide Stimulation. *Int J Mol Sci*. 2021;22(16):8877. doi:10.3390/ijms22168877
35. Huang X, Qiu W, Pan Y, et al. Exosomes from LPS-Stimulated hDPSCs Activated the Angiogenic Potential of HUVECs In Vitro. *Stem Cells Int*. 2021;2021:6685307. doi:10.1155/2021/6685307
36. Wu M, Liu X, Li Z, et al. SHED aggregate exosomes shuttled miR-26a promote angiogenesis in pulp regeneration via TGF-beta/SMAD2/3 signalling. *Cell Prolif*. 2021;54(7):e13074. doi:10.1111/cpr.13074
37. Sato M, Toriumi T, Watanabe N, et al. Characterization of mesenchymal progenitor cells in crown and root pulp from human mesiodentes. *Oral Dis*. 2015;21(1):e86–97. doi:10.1111/odi.12234
38. Ge L, Xun C, Li W, et al. Extracellular vesicles derived from hypoxia-preconditioned olfactory mucosa mesenchymal stem cells enhance angiogenesis via miR-612. *J Nanobiotechnology*. 2021;19(1):380. doi:10.1186/s12951-021-01126-6
39. Xian X, Gong Q, Li C, Guo B, Jiang H. Exosomes with Highly Angiogenic Potential for Possible Use in Pulp Regeneration. *J Endod*. 2018;44(5):751–758. doi:10.1016/j.joen.2017.12.024
40. Li B, Xian X, Lin X, et al. Hypoxia Alters the Proteome Profile and Enhances the Angiogenic Potential of Dental Pulp Stem Cell-Derived Exosomes. *Biomolecules*. 2022;12(4):575. doi:10.3390/biom12040575
41. Wu J, Chen L, Wang R, et al. Exosomes Secreted by Stem Cells from Human Exfoliated Deciduous Teeth Promote Alveolar Bone Defect Repair through the Regulation of Angiogenesis and Osteogenesis. *ACS Biomater Sci Eng*. 2019;5(7):3561–3571. doi:10.1021/acsbiomaterials.9b00607
42. Akhtar N, Dickerson EB, Auerbach R. The sponge/Matrigel angiogenesis assay. *Angiogenesis*. 2002;5(1–2):75–80. doi:10.1023/a:1021507031486
43. Aref Z, Quax PHA. In Vivo Matrigel Plug Assay as a Potent Method to Investigate Specific Individual Contribution of Angiogenesis to Blood Flow Recovery in Mice. *Int J Mol Sci*. 2021;22(16):8909. doi:10.3390/ijms22168909
44. Liu P, Qin L, Liu C, et al. Exosomes Derived From Hypoxia-Conditioned Stem Cells of Human Deciduous Exfoliated Teeth Enhance Angiogenesis via the Transfer of let-7f-5p and miR-210-3p. *Front Cell Dev Biol*. 2022;10:879877. doi:10.3389/fcell.2022.879877
45. Ge X, Li Z, Jing S, et al. Parathyroid hormone enhances the osteo/odontogenic differentiation of dental pulp stem cells via ERK and P38 MAPK pathways. *J Cell Physiol*. 2020;235(2):1209–1221. doi:10.1002/jcp.29034
46. Rode B, Bailey MA, Marthan R, Beech DJ, Guibert C. Orai Channels as Potential Therapeutic Targets in Pulmonary Hypertension. *Physiology*. 2018;33(4):261–268. doi:10.1152/physiol.00016.2018
47. Wang S, Xu L, Wu Y, et al. Parathyroid Hormone Promotes Human Umbilical Vein Endothelial Cell Migration and Proliferation Through Orai1-Mediated Calcium Signaling. *Front Cardiovasc Med*. 2022;9:844671. doi:10.3389/fcvm.2022.844671
48. Gu C, Lhamo T, Zou C, et al. Comprehensive analysis of angiogenesis-related genes and pathways in early diabetic retinopathy. *BMC Med Genomics*. 2020;13(1):142. doi:10.1186/s12920-020-00799-6

49. Paik JY, Ko BH, Jung KH, Lee KH. Fibronectin stimulates endothelial cell 18F-FDG uptake through focal adhesion kinase-mediated phosphatidylinositol 3-kinase/Akt signaling. *J Nucl Med*. 2009;50(4):618–624. doi:10.2967/jnumed.108.059386
50. Chen J, Zhang X, Liu X, et al. Ginsenoside Rg1 promotes cerebral angiogenesis via the PI3K/Akt/mTOR signaling pathway in ischemic mice. *Eur J Pharmacol*. 2019;856:172418. doi:10.1016/j.ejphar.2019.172418